Nanoscale

PAPER

View Article Online
View Journal | View Issue

Cite this: *Nanoscale*, 2025, **17**, 28023

Ligand-controlled Fe_3O_4 nanoparticles as reusable adsorbents for dye removal in the chemical recycling of coloured polyester textiles

Hyein Hwang,[a,b] Minchang Kim,[a] Seohyun Kim,[c] Yongjoon Kim,[a,d] Minwoo Han,[e] Megalamane S. Bootharaju,[f,g] Munhong Min,[e] Taeghwan Hyeon *[f,g] and Byung Hyo Kim *[a,b,d]

Received 11th September 2025,
Accepted 18th November 2025

DOI: 10.1039/d5nr03835a

rsc.li/nanoscale

Chemical recycling of polyester through depolymerisation processes is a promising strategy to mitigate the environmental burden of polyester-containing textile waste. However, residual disperse dyes in depolymerised products often degrade the purity and whiteness of recovered monomers. Conventional dye removal methods, such as solvent extraction, frequently fail to achieve complete dye removal. Herein, we report the development of iron oxide magnetic nanoadsorbents capped with three hydrophobic ligands for the efficient removal of disperse dyes from monomer solutions. Strong hydrophobic interactions between the ligands and dye molecules significantly enhance adsorption efficiency. Systematic evaluation with different dyes reveals that molecular features such as contour length, polarisability, and flexibility strongly influence adsorption performance. The dye-adsorbed nanoadsorbents are readily recovered through magnetic separation and reused without structural degradation. By applying the nanoadsorbents to the decolourisation of depolymerised coloured textiles, we obtained highly pure white monomers suitable for repolymerisation into textile-grade materials. These findings highlight a sustainable and reusable nanomaterial platform for dye removal during the recycling of polyester textiles.

Introduction

Global polyester textile production is increasing annually, reaching 74 million tonnes in 2022, and accounts for more than half of the total textile market owing to its superior properties, such as excellent tensile resistance, wash fastness, and abrasion resistance.[1] The mass production of polyester-based fibres has resulted in a substantial amount of discarded textiles. At present, textile waste is mainly managed through landfilling or incineration, which not only causes soil and air pollution but also depletes available resources in the textile value chain.[2,3]

Recycling or upcycling polyester-based textile waste into high-value pure fibres is considered a feasible solution to address the associated environmental issues, particularly for polyethylene terephthalate (PET) fibres. Waste polyester fibres can be recycled *via* chemical recycling, where the polymer is depolymerised into monomers and subsequently repolymerised.[4] Nucleophilic solvents, such as ethylene glycol, water, and methanol, are commonly employed for depolymerisation through nucleophilic substitution of the ester bonds in polyester chains.[5] Among these approaches, ethylene glycol-based depolymerisation, known as glycolysis, has emerged as a promising methodology due to its mild reaction conditions and cost-effectiveness.[6,7]

When applying glycolysis to polyester-containing textiles, the influence of dyes on both process controllability and product purity must be carefully considered.[3] Dye molecules in coloured polyester can induce undesirable side reactions, reduce the intrinsic viscosity of polyester chips, yield low-value recycled polyester, and even pollute the working environment during recycling. Furthermore, dyes that remain after the recycling process can cause unpredictable coloration in recycled products, thereby decreasing the market value of textiles produced from recycled fibres with undesired colours.[2,8,9] Therefore, dye removal constitutes a critical step in fibre-to-fibre recycling.

[a]*Department of Materials Science and Engineering, Soongsil University, Seoul 06978, Republic of Korea. E-mail: byunghyokim@ssu.ac.kr*
[b]*Department of Convergence of Energy Policy and Technology, Soongsil University, Seoul 06978, Republic of Korea*
[c]*Department of Chemistry, Soongsil University, Seoul 06978, Republic of Korea*
[d]*Department of Green Chemistry and Materials Engineering, Soongsil University, Seoul 06978, Republic of Korea*
[e]*DYETEC Institute, Daegu 41706, Republic of Korea*
[f]*Center for Nanoparticle Research, Institute for Basic Science (IBS), Seoul 08826, Republic of Korea*
[g]*School of Chemical and Biological Engineering, and Institute of Chemical Processes, Seoul National University, Seoul 08826, Republic of Korea*

The conventional method for removing dyes from textile waste is solvent extraction, in which dye molecules are removed using appropriate solvents. Solvents with solubility parameters and polarity similar to those of dye molecules, such as *N*,*N*-dimethylformamide, dimethyl sulfoxide, chlorobenzene, chloroform, acetic acid, and ethylene glycol, are commonly employed for dye extraction with high throughput.[8,10,11] However, this method cannot completely eliminate residual dyes inside fibres because the process is governed by the equilibrium partitioning of dyes between the fibre and solvent.[2,12] At equilibrium, the dye concentrations in the fibre and solvent balance, leaving a significant proportion of dye molecules in the textile. Furthermore, strong dye–polymer interactions substantially reduce extraction efficiency. Due to their high stability within the dense fibre matrix, dye molecules tend to remain inside the fibres rather than migrate into the solvent.[13] In particular, for polyester textiles that use disperse dyes containing azo or anthraquinone groups, the hydrophobic dye molecules are strongly encapsulated in the amorphous regions of the polyester, making their removal especially difficult.[14] Continuous solvent infusion has been attempted to enhance dye extraction efficiency; however, this approach requires a large amount of solvent, thereby resulting in high cost and additional environmental burdens.[15]

An additional dye removal step for polyester textiles is therefore required to eliminate residual dye molecules. After depolymerisation of the polymer chains into monomers, dyes that are previously trapped in the amorphous regions of polyester fibres become unencapsulated, enabling their removal by adsorption using adsorbents such as activated carbon.[16,17] Although activated carbon exhibits strong adsorption capacity for disperse dyes, its application has largely been limited to wastewater treatment and has not been widely adopted for dye removal after chemical recycling owing to selectivity issues and desorption challenges.[18] For instance, bis(2-hydroxyethyl) terephthalate (BHET), a product of PET chemical recycling, is also adsorbed within the pores of activated carbon *via* π–π interactions, leading to significant production losses.[1] Moreover, desorption of adsorbed dyes requires substantial time and energy, thereby increasing the cost of adsorbent regeneration.[1,19] Therefore, the development of selective adsorbents suitable for chemical recycling of waste fibres is urgently required.

In this study, we developed selective dye removal agents based on dispersible superparamagnetic nanoparticles. Using these nanoparticles, we eliminated 83% of residual dyes from the solution and recovered the dyes after magnetic separation. Through ligand engineering of the magnetic nanoparticles, we investigated the influence of the ligand structure and chain length on the adsorption properties of various dyes. Employing this adsorbent, we extracted dyes from coloured chemically recycled products and subsequently obtained white monomers (L^* = 71.51, a^* = 3.13, b^* = 2.83) from depolymerised PET. These results suggest a potential solution to the problem of residual dyes, which constitute a major bottleneck in the chemical recycling of coloured fibres.

Results and discussion

Characterisation of nanoparticles

We prepared three types of iron oxide nanoparticles capped with different ligands (oleate, stearate, and laurate) *via* thermal decomposition of $Fe(acac)_3$ precursors at 290 °C in benzyl ether solvent in the presence of each ligand.[20–22] TEM images of the oleate-, stearate-, and laurate-capped iron oxide nanoparticles show high monodispersity with sizes ranging from 6.6 nm to 7.1 nm (Fig. 1a–c). Successful encapsulation of the ligands was confirmed by Fourier transform infrared (FT-IR) spectra of the synthesised nanoparticles (Fig. 1d and Fig. S1). Peaks at 2927 cm^{-1} and 2857 cm^{-1} observed for all three types of nanoparticles correspond to the asymmetric and symmetric C–H stretching modes of the hydrocarbon chains of the ligands, confirming effective ligand passivation on the nanoparticle surfaces.[23,24] Small differences in the IR spectra reflect structural variations among the ligands. For instance, a peak at 3004 cm^{-1} in oleate-capped nanoparticles indicates the presence of C=C double bonds, as this peak is characteristic of C–H vibrations in unsaturated bonds.[25] A shoulder peak at 2960 cm^{-1} for laurate-capped nanoparticles corresponds to C–H stretching of primary carbons, which is attributed to the higher proportion of primary carbons in laurate (carbon number = 12) compared with oleate and stearate (carbon number = 18).[26]

The crystal structures of the synthesised iron oxide nanoparticles were analysed using XRD. The peaks at 30°, 34°, 42°, 53°, 56°, and 62° matched well with the (220), (311), (400), (422), (511), and (440) planes of magnetite (Fe_3O_4) with a spinel structure, confirming that the oleate-, stearate-, and laurate-capped nanoparticles are magnetic materials.[27,28] Their magnetic properties were characterised under an applied magnetic field (H) ranging from −1.5 T to 1.5 T at room temperature. All nanoparticles exhibited high saturation magnetisation of 50–60 emu g^{-1}, indicating that they can be efficiently recovered with external magnets after dye adsorption.[29] The negligible coercivity and remanence of the nanoparticles, attributed to their nanoscale domain structures, ensure that the nanoparticles remain well-dispersed in media.[30,31]

Decolourisation of disperse dye solution

We applied the three types of Fe_3O_4 nanoparticles capped with hydrophobic ligands as adsorbents to remove residual dye molecules and produce highly pure recycled products from waste polyester textiles. Most polyester clothing contains disperse dyes, which are generally categorised as conjugated molecules containing azo or anthraquinone groups.[32] In this study, conventional azo and anthraquinone dyes with identical hues, Disperse Red 1 and Disperse Red 60, were selected as model systems to test the applicability of the method to different chromophores (Fig. 2). In addition, two conventional anthraquinone dyes with different hues, Disperse Blue 56 and Disperse Yellow 54, were chosen to investigate structural effects (Fig. 2). For simplicity, these four conventional dyes are hereafter referred to as DR1, DR60, DB56, and DY54.

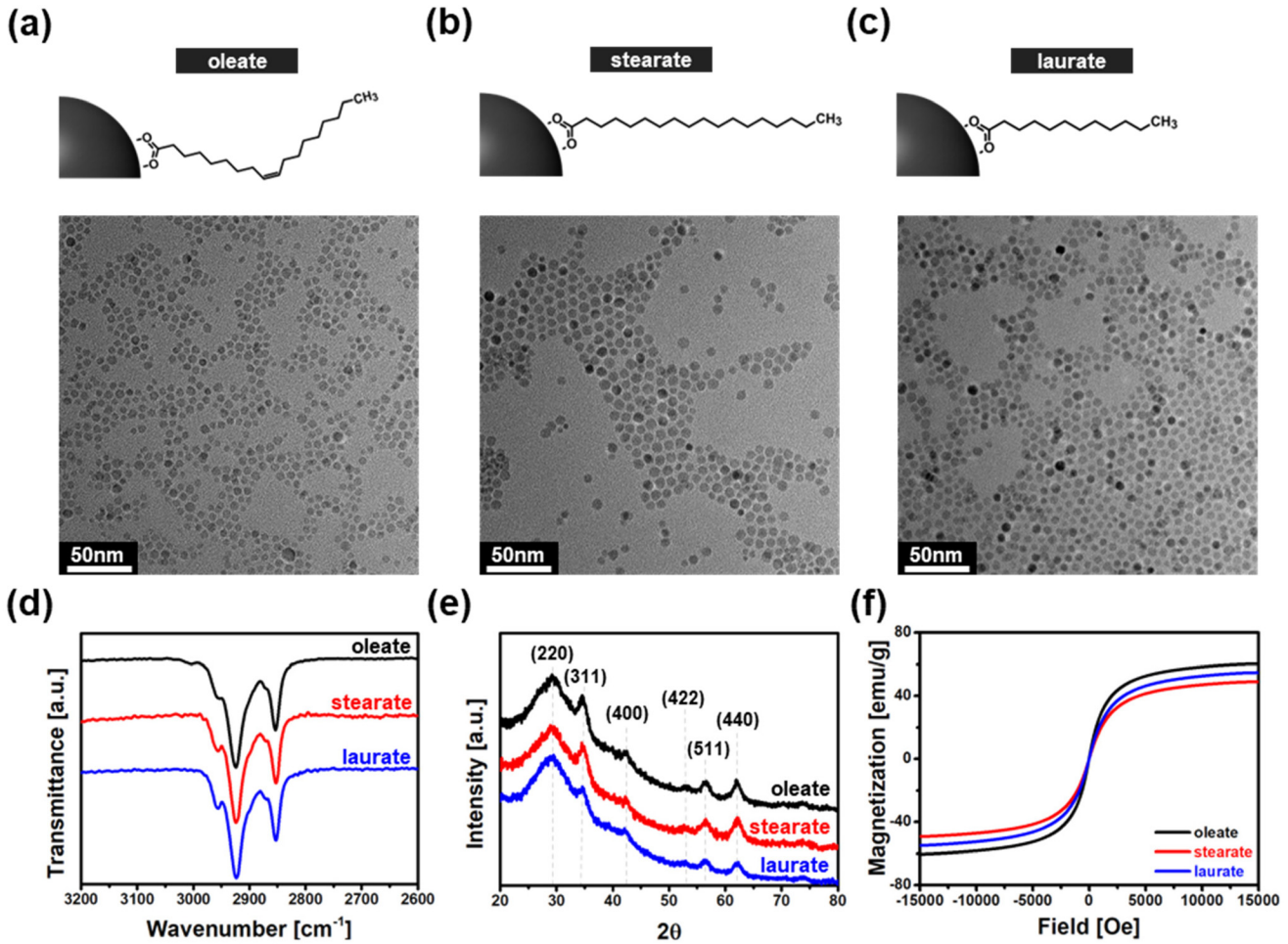

Fig. 1 Structural characterisation of Fe_3O_4 nanoparticles capped with different ligands: (a–c) Schemes (top) and TEM images (bottom) of oleate-, stearate-, and laurate-capped nanoparticles, respectively; (d) FT-IR spectra; (e) XRD patterns; and (f) VSM curves.

Dye removal experiments were performed using nanoadsorbents capped with three types of ligands: oleate, stearate, and laurate. Both stearate and oleate ligands contain 18 carbon atoms and have similar contour lengths, but their structures differ: the *cis*-C=C double bond in the oleate ligand induces a bent conformation, whereas stearate has a linear conformation. Laurate ligands, on the other hand, have a shorter chain length of 12 carbons, corresponding to a shorter contour length of 14.9 Å compared with the 22.1 Å for stearate.

Before applying the nanoparticle adsorbents to depolymerised waste polyester textiles, we quantitatively analysed their adsorption properties using model dye solutions. To simulate the conditions after the glycolysis reaction, the initial dye concentration was set at 30 μmol L^{-1}, and the solvent system was modelled with 1 : 9 ethylene glycol to water. The amount of adsorbent was fixed at 1 g L^{-1}. Using the three types of ligand-capped nanoadsorbents and the four selected disperse dyes, we examined the effects of ligand structures and dye–ligand interactions on dye removal efficiency.

Dye removal efficiencies were quantitatively measured using calibrated UV-vis spectroscopy (Fig. 2 and Fig. S2). For DR60 dye, stearate- and oleate-capped nanoparticles removed 83.1% and 63.4% of dye molecules from solution, respectively. The high removal efficiency arises from hydrophobic–hydrophobic interactions between the long chain hydrophobic ligands of nanoparticles and the non-ionic disperse dyes.[33] In contrast, laurate-capped nanoparticles, with a shorter carbon chain length (C12), removed only 26.2% of the DR60 dye, much lower than that observed for nanoparticles capped with long-chain ligands (C18) (Fig. 2).

Interestingly, the removal trends varied depending on the dye molecules. For DR1, the laurate-capped nanoparticles exhibited the highest removal rate (48.7%), while the oleate- and stearate-capped nanoparticles showed removal rates of 44.6% and 45.1%, respectively. DB56 was relatively poorly removed, with efficiencies of 20.8%, 23.0%, and 11.1% for oleate-, stearate-, and laurate-capped nanoparticles, respectively, which are significantly lower than those for DR60 and DR1. Similarly, DY54 removal efficiencies were limited to 25.8%, 22.9%, and 13.3% for nanoadsorbents capped with oleate, stearate, and laurate, respectively. Taken together, the optimal dye–ligand combinations are laurate-capped nanoad-

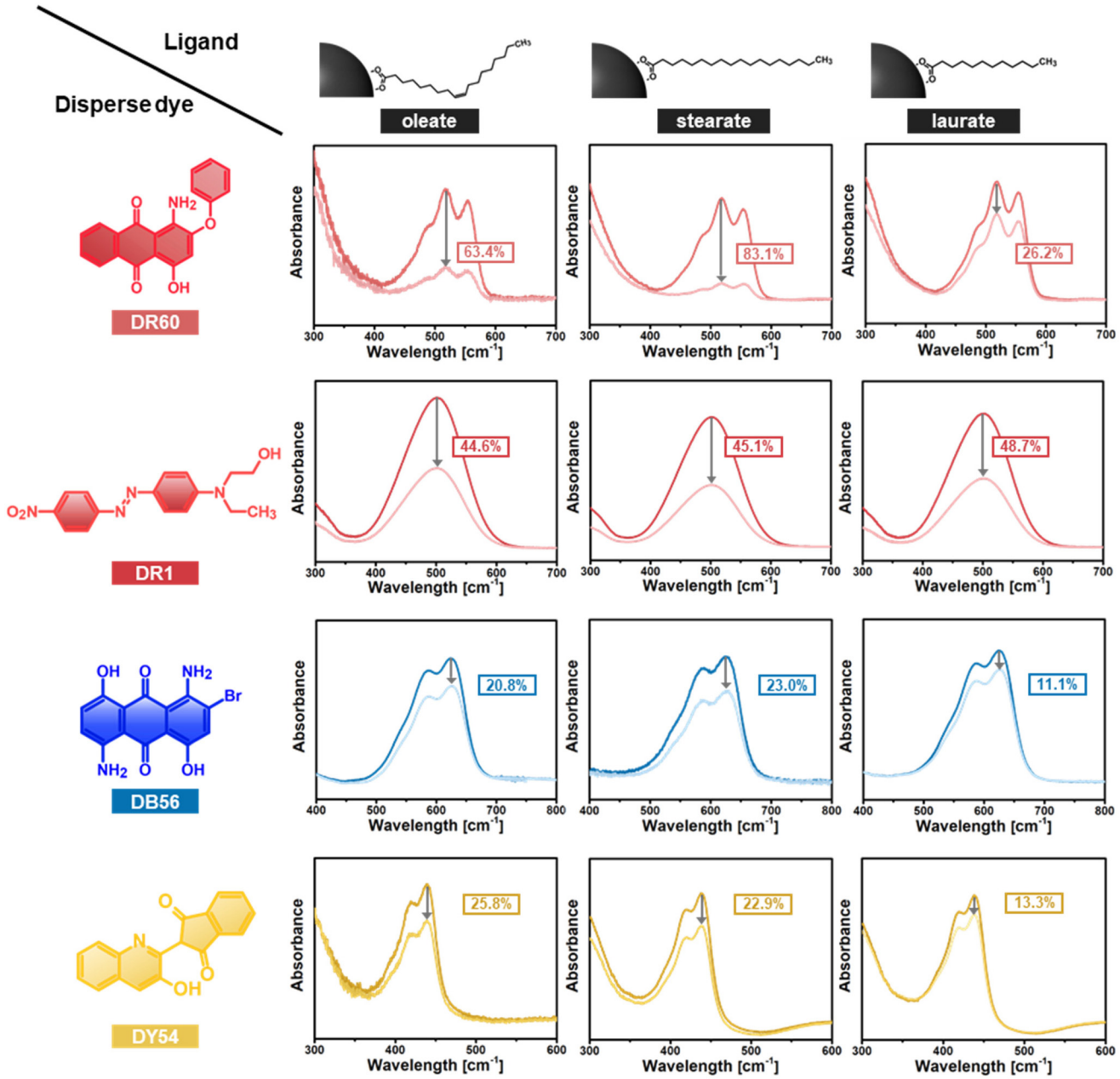

Fig. 2 Changes in the UV-vis absorption spectra and decolourisation efficiencies of Fe_3O_4 nanoparticles capped with different ligands (oleate, stearate, and laurate) towards four commercial disperse dyes (DR60, DR1, DB56, and DY54).

sorbents for DR1, stearate-capped nanoadsorbents for DR60 and DB56, and oleate-capped nanoadsorbents for DY54.

Effect of ligand selectivity and dye structure

We next investigated how the interplay between ligand characteristics[34,35] and dye molecular structures[36] (Fig. 3a) governs decolourisation efficiency. To analyse the correlation between ligand types and dye structures, six molecular parameters of the dye molecules were considered: end-to-end distance, contour length, width, linearity, molar volume, and polarizability (Fig. 3b and Table 1). Molar volume and polarizability values were obtained from databases,[37–40] whereas the other structural parameters were measured from three-dimensional molecular models (Fig. S3).[41,42] The dependence of these factors on the decolourisation rates for the three ligand-capped nanoparticles is shown in Fig. 3c–e.

The decolourisation efficiency was positively correlated with polarizability. The polarizability reflects how easily the electron cloud of a molecule can be distorted by an external electric field, and this distortion underlies van der Waals interactions.[43,44] Accordingly, greater polarizability strengthens ligand–dye interactions and improves dye removal efficiency.

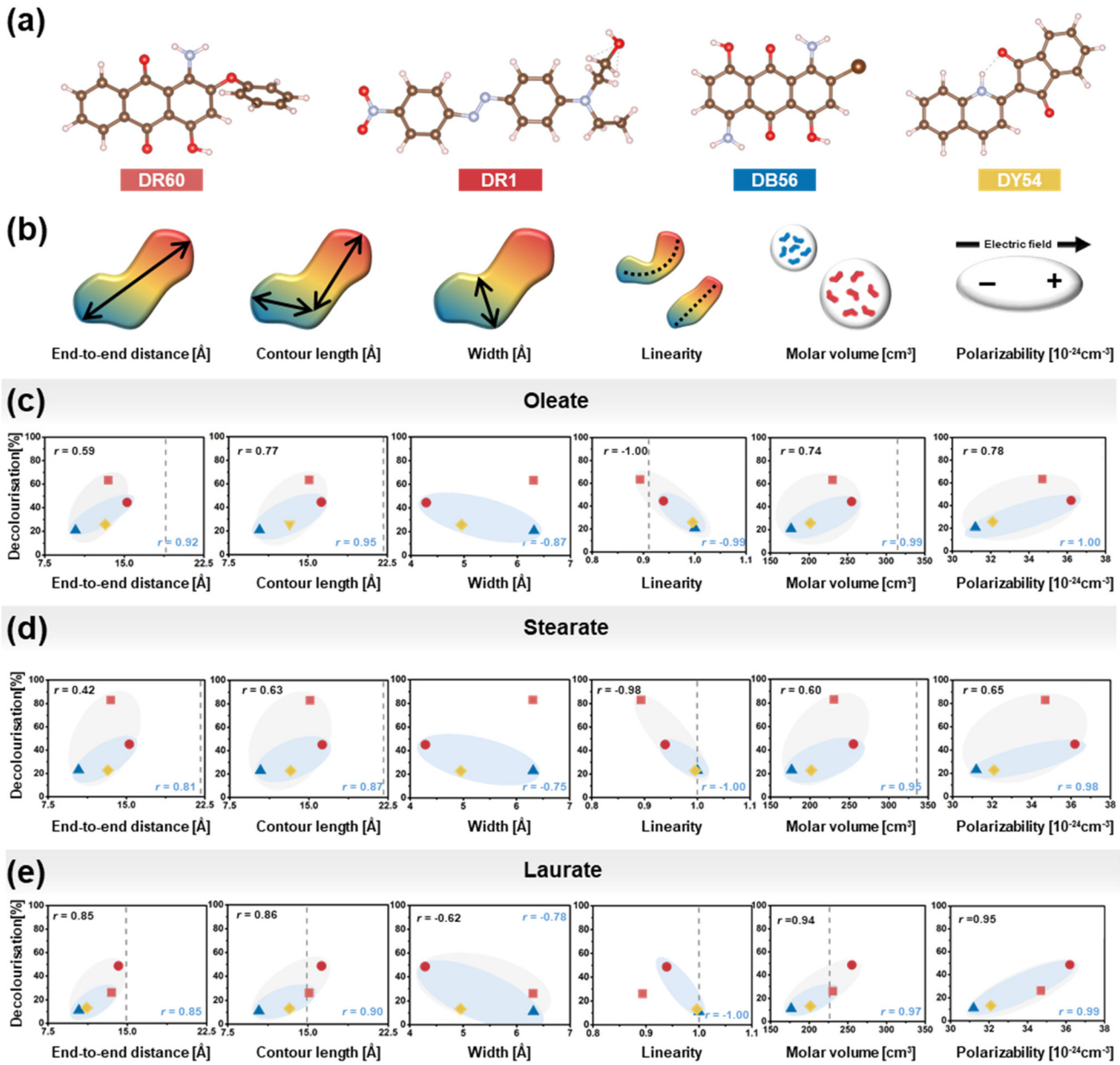

Fig. 3 (a) Three-dimensional structures of four disperse dyes; (b) diagram of six defined molecular parameters; and (c–e) decolourisation performance as a function of these parameters (red square: DR60, red circle: DR1, blue triangle: DB56, and yellow diamond: DY54).

Table 1 Six defined molecular parameters of four commercial disperse dyes (DR60, DR1, DB56, and DY54)

	DR60	DR1	DB56	DY54
End-to-end distance [Å]	13.50	15.27	10.41	13.21
Contour length [Å]	15.11	16.26	10.41	13.27
Width [Å]	6.31	4.29	6.31	4.95
Linearity	0.893	0.939	1	0.997
Molar volume [cm^3]	255.1 ± 7.0	230.4 ± 3.0	201.5 ± 3.0	176.7 ± 3.0
Polarizability [10^{-24} cm^{-3}]	34.7 ± 0.5	36.2 ± 0.5	32.1 ± 0.5	31.2 ± 0.5

The polarizability effect also explains the relatively poor performance of the laurate-capped nanoparticles, as the low polarizability of laurate leads to weaker van der Waals interactions with dye molecules.

Polarizability is closely correlated with molar volume; thus, the molar volume of a dye follows a similar trend to its polarizability.[45] The molar volume component can be further divided into a length contribution (end-to-end distance) and a width contribution. For oleate-, stearate-, and laurate-capped nanoadsorbents, the end-to-end distance was positively correlated with the decolourisation efficiency, with the correlation coefficients (r values) of 0.59, 0.42, and 0.85, respectively. This

suggests that longer dye molecules interact more effectively with the ligand shell.

In contrast, the effect of molecular width depends on ligand type. For laurate-capped nanoadsorbents, decolourisation efficiency decreased with increasing dye width, whereas no clear trend was observed for oleate- and stearate-capped nanoadsorbents. This can be attributed to the spacing between ligands coordinated on nanoparticle surfaces. Considering the typical surface density of carboxylate ligands on Fe_3O_4 nanoparticles (3.5–4 nm^{-2}),[46] the longer oleate and stearate ligands create sufficient spacing to accommodate bulky dye molecules, whereas the shorter laurate ligands hinder the insertion of large dye molecules (Fig. S4). As a result, dye width becomes a limiting factor for laurate-capped nanoadsorbents.

We further investigated the decolourisation performance with respect to contour length, defined as the total molecular length considering bond lengths and angles in the molecular chain. The contour length showed a trend similar to that of the end-to-end distance. We also examined the effect of molecular shape by considering linearity, defined as the ratio between the end-to-end distance and contour length. Dyes with low linearity tend to show high decolourisation rates.

DR60 deviates from these linear correlations (Fig. 3c–e) with an exceptionally high removal rate. The behavior is attributable to conformational flexibility about its aryl–O–aryl ether bond, which has a very low rotational energy barrier (0.36–0.40 kcal mol^{-1}; Table S1).[47–49] This flexibility around the ether bond enables dye molecules to intercalate between ligands. Consequently, the flexible DR60 exhibited particularly high dye removal rates compared with the other dyes.

With the exception of DR60, DR1 (an aromatic molecule linked by an aromatic azo group), DB56 (a polycyclic aromatic molecule), and DY54 (a quinophthalone dye that predominantly exists in the enaminone (NH-form) tautomer with a high rotation barrier, 15.5 kcal mol^{-1}; see Table S1)[50] can be regarded as rigid molecules. When analysis was restricted to these three rigid dyes (DR1, DB56, and DY54), the trends between molecular parameters and decolourisation rates became much clearer. The r values obtained for the rigid dyes (shown in blue in Fig. 3c–e) were substantially higher than those obtained for all four dyes (shown in black). For example, for oleate-capped nanoadsorbents, the correlation between molar volume and the decolourisation rate yielded an r value of 0.74 across all four dyes, but this increased to 0.99 when restricting the analysis to the three rigid dyes. Likewise, the correlations with decolourisation rates for most parameters exceeded r = 0.9 for rigid dyes. Thus, rigid dye molecules with large polarizability and elongated shapes exhibit predictable and enhanced decolourisation efficiency.

Decolourisation of depolymerised monomers from coloured textiles

Building on the adsorption performance of the nanoadsorbents in dye solutions, we carried out dye removal during the chemical recycling of polyester textiles. We applied the nanoadsorbents in the glycolysis process of PET textiles, the dominant polyester type. Specifically, the dye was preliminarily extracted with a solvent from PET fibres dyed with DR60 before depolymerisation. As shown in Fig. 4 (top), the dye was not completely removed during this preliminary extraction step. The partially decolourised fibres were then depolymerised to yield BHET monomers that still contained residual dye. Without an additional dye removal step, the residual dye may act as a nucleation seed around which BHET crystallised. Consequently, the dye may become encapsulated in the BHET crystals, leading to the precipitation of coloured BHET.[51]

Therefore, dye removal after the depolymerisation process is essential.

In this study, we successfully removed the residual dye in BHET using nanoadsorbents and obtained pure white BHET. UV-vis absorption measurements showed a significant decrease in absorbance at 509 nm after nanoadsorbent treatment, confirming efficient dye removal during the secondary decolourisation process (Fig. 4a). In addition, the colour difference of BHET before and after decolourisation was quantified using a whiteness meter. The chromaticity coordinates were defined by relative ratios of the CIE 1931 tristimulus values $\left(x = \frac{X}{X+Y+Z}, y = \frac{Y}{X+Y+Z}\right)$.[52] Accordingly, the coordinates shifted from (0.3227, 0.2945) before decolourisation to (0.3255, 0.3349) after decolourisation (Fig. 4b). Also, the L^*, a^*, and b^* values changed from 75.09 to 71.51, from 19.40 to 3.13 and from −10.36 to 2.83, respectively, after decolourisation (Fig. 4c). The decrease in the a^* (red–green) component towards zero indicates that the red DR60 dye was almost completely eliminated. Importantly, the whiteness values also imply that the dark brown nanoadsorbents were magnetically separated and rarely remained in the depolymerised BHET. Together, these results establish our nanoadsorbent-assisted decolourisation as an effective strategy for producing high-purity monomers from depolymerised coloured polyester textiles.

Recovery of nanoadsorbents

The reusability of nanoadsorbents is crucial for ensuring their economic viability and practical applicability. In this context, it is essential that their structural integrity is preserved after repeated cycles of dye adsorption and desorption. FT-IR analysis confirmed the retention of the ligands before and after adsorption experiments. Identical IR peaks representing the asymmetric and symmetric C–H stretching modes of the ligands were observed at 2927 cm^{-1} and 2857 cm^{-1} (Fig. 5a and Fig. S5).[23,24] This result indicates that the ligand structure remained intact and capped to the nanoparticle surface during dye adsorption and desorption. XRD analysis revealed that both fresh and recovered nanoadsorbents are magnetite with a spinel structure (Fig. 5b).[27,28] Thus, the nanoadsorbents retained their crystalline and magnetic properties after recovery, ensuring efficient magnetic separation and reuse.

We then assessed the reuse of the oleate-capped Fe_3O_4 adsorbent. Under identical conditions, the decolourisation ratio decreased from 63.4% in cycle 1 to 32%, 26%, and 23.4%

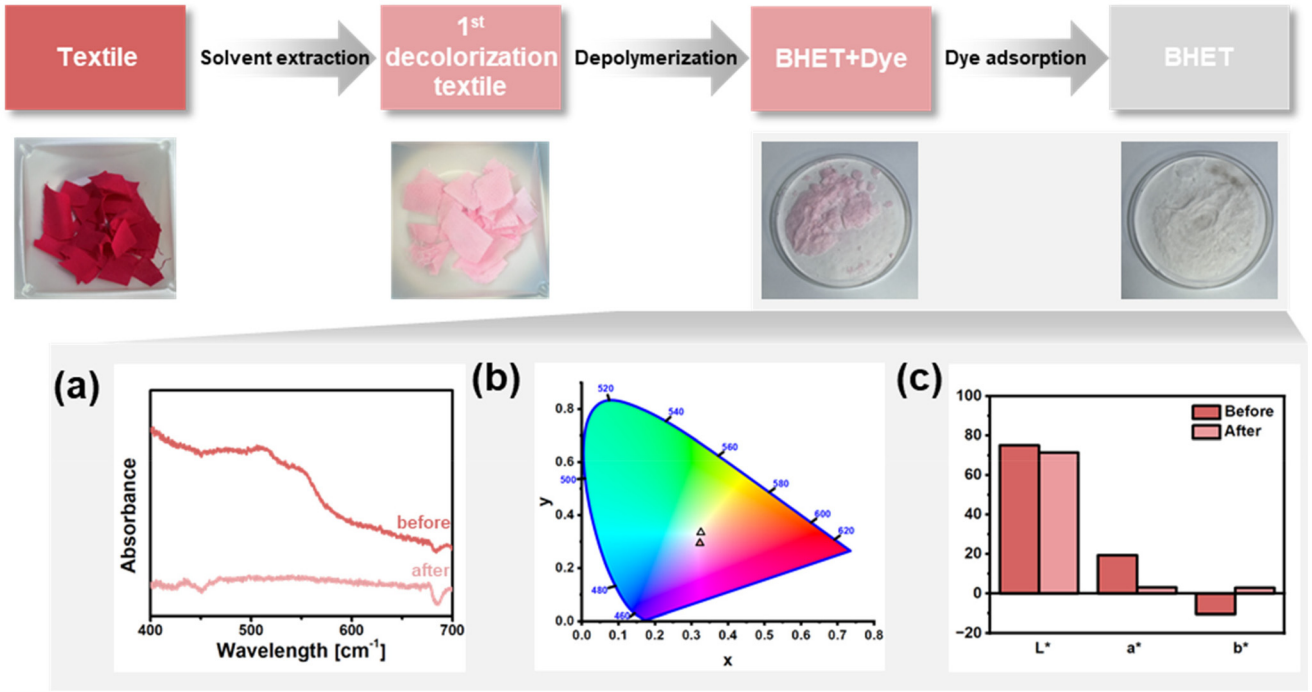

Fig. 4 Schematic of the first and second decolourisation steps (top) of commercial coloured fibres. (a) UV-vis absorption spectra; (b) CIE chromaticity of BHET; and (c) L^*, a^*, and b^* values from colorimetric analysis, showing comparison of results before and after the second decolourisation.

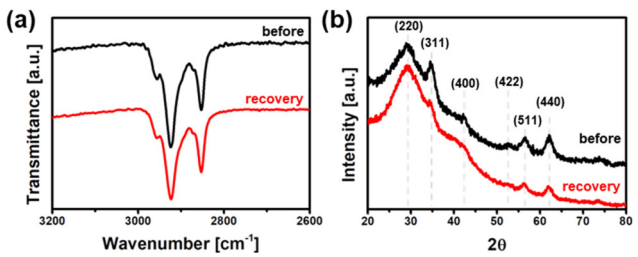

Fig. 5 Structural analysis of Fe_3O_4 nanoparticles before dye removal and after recovery: (a) FT-IR spectra and (b) XRD patterns.

in cycles 2–4, respectively (Fig. S6). The decline is attributable to incomplete desorption and site fouling rather than structural degradation, as supported by the spectroscopic and diffraction data. Improving the regeneration step, for example, tuning the extraction-solvent polarity and applying mild ultrasonication, is expected to enhance reusability and will be pursued in future work.

Conclusions

In summary, Fe_3O_4 nanoparticles capped with fatty acid ligands (oleate, stearate, and laurate) were synthesised and applied as nanoadsorbents for disperse dye removal. Their ligand-dependent adsorption behaviour enabled efficient decolourisation, with performance strongly influenced by the interplay between ligand type and dye structure. The nanoadsorbents maintained structural integrity and reusability after dye adsorption and desorption, confirming their robustness. Relative to conventional wastewater adsorbents (*e.g.*, activated carbon or polymer/clay composites) that rely on hydrophobic/π–π interactions, our approach benchmarks a similar interaction paradigm in the BHET/EG post-depolymerisation matrix and couples it with rapid magnetic retrieval, enabling minute-scale decolourisation without filtration or centrifugation. This study demonstrated that stearate-capped Fe_3O_4 nanoparticles achieved removal efficiencies of up to 83% for the DR60 dye. The adsorption-based approach presented in this study can be further enhanced by combining it with established dye degradation technologies, such as photolysis, redox reactions, and electrolysis, to achieve near-complete dye removal.[53–55] This methodology is broadly applicable and it can be extended to various processes and technologies. This ligand-engineering strategy provides an effective route for extending chemical recycling from colourless to coloured PET fibres, thereby broadening the scope of sustainable polyester recycling and advancing nanoscale solutions for circular textile technologies.

Experimental

Materials

1,2-Hexadecanediol (98%), iron(III) acetylacetonate ($Fe(acac)_3$, 99.9%), benzyl ether (98%), oleic acid (90%), oleylamine (70%), lauric acid (98%), dodecylamine, stearic acid (98%), and stearylamine (85%) were purchased from Sigma-Aldrich

(St Louis, MO, USA). Zinc acetate was obtained from Rhawn (Shanghai, China), and ethylene glycol (99.5%) was purchased from Duksan (Ansan, Republic of Korea).

Synthesis of ligand-capped Fe_3O_4 nanoparticles

$Fe(acac)_3$ (2 mmol), 1,2-hexadecanediol (10 mmol), a long-chain hydrocarbon acid (6 mmol), and a long-chain hydrocarbon amine (6 mmol) were mixed and stirred under an argon flow. Oleic acid/oleylamine, stearic acid/stearylamine, and lauric acid/dodecylamine pairs were employed as the respective capping agents to obtain oleate-, stearate-, and laurate-capped nanoparticles. The mixture was degassed under vacuum at 100 °C for 1 h, heated to 290 °C at a rate of 4 °C min^{-1}, and refluxed for 30 min. After removal of the heat source, the dark brown dispersion was cooled to room temperature. The resulting product was precipitated with ethanol, centrifuged to remove the solvent, and redispersed in hexane.

Removal of dyes from dye solution

An experiment was conducted to simulate the conditions after PET glycolysis. A dye solution was prepared by dissolving the dye in ethylene glycol at a concentration of 300 μM L^{-1}, followed by mixing with deionised water at a 1 : 9 volume ratio. The adsorbent was dried and subsequently redispersed in pentane at a concentration of 10 g L^{-1}. At room temperature, 5 mL of the glycolysis-simulated dye solution was mixed with 0.1 mL of the nanoadsorbent suspension. The mixture was dried for 30 min to form Fe_3O_4 flakes, after which dye removal was performed by vortexing for 10 min. The adsorbent was then separated from the dye solution by magnetic separation, and ethanol was added to the supernatant. The residual dye concentration was determined using ultraviolet-visible (UV-vis) spectroscopy.

The decolourisation efficiency (R) was calculated according to the following equation:

$$R\,(\%) = \frac{(C_i - C_e)}{C_i} \times 100$$

where C_i and C_e are the initial and equilibrium dye concentrations (μM L^{-1}), respectively. Six parameters were defined for the dyes, and their effect on removal efficiency was analysed. The correlation coefficient (r value) was calculated according to the Pearson correlation equation to evaluate the linear relationship between the measured and fitted values.

PET fibre dyeing with commercial dyes

A dye solution was prepared at a concentration of 1% o.w.f of Disperse Red 60 with a liquor ratio of 1 : 1. The prepared solution and ISO ADJ polyester standard fabric were placed in a 200 mL high-pressure pot of an infrared dyeing machine and mounted on a Mathis AG IR dyeing machine (LABOMAT BFA). The temperature was then increased to 140 °C at a heating rate of 3 °C min^{-1}, maintained at 140 °C for 40 min, and subsequently cooled to 60 °C at a rate of 4 °C min^{-1}.

To remove unfixed dye, a reduction clearing bath was prepared by dissolving NaOH (3 g L^{-1}) and $Na_2S_2O_4$ (5 g L^{-1}) in water. The reduction clearing process was subsequently carried out at 60 °C for 20 min.

Coloured PET fibre decolourisation

Preliminary decolourisation of PET fibres (1 g) dyed with Disperse Red 60 (1% o.w.f.) was conducted by extracting dye molecules into 40 mL of ethylene glycol with vigorous stirring at 196 °C for 30 min. This preliminary decolourisation step was repeated twice. The partially decolourized fibres were subsequently washed with deionised water.

The decolourized fibres were depolymerised *via* catalytic glycolysis using zinc acetate as a catalyst. Specifically, 1 g of decolourized PET fibre, 0.01 g of zinc acetate, and 20 mL of ethylene glycol were placed in a three-neck round-bottom flask. The mixture was degassed under vacuum at 70 °C for 1 h and then heated to 180 °C at a rate of 4 °C min^{-1} under an argon flow. The glycolysis reaction was carried out at this temperature for 2 h.

The second decolourisation was performed concurrently with the recrystallisation of monomers after glycolysis. Following the reaction, 0.02 g of Fe_3O_4 nanoadsorbents and 180 mL of preheated deionised water were added to the depolymerised solution. The mixture was vortexed for 10 min to ensure adsorption of dyes onto the adsorbents. The dye-adsorbed Fe_3O_4 adsorbents were then separated using magnets. After dye removal, the purified solution was stored at 4 °C overnight, yielding BHET crystals by precipitation. The dye-containing nanoadsorbents were regenerated by treatment with acetone to desorb the dye molecules, followed by magnetic separation to recover the Fe_3O_4 powder.

Characterization of materials

Transmission electron microscopy (TEM) was performed using a Talos F200X G2 instrument (Thermo Fisher Scientific, MA, USA) operated at an accelerating voltage of 200 kV. Structural characterization was carried out using X-ray diffraction (XRD; D2 Phase, Bruker, Ettlingen, Germany). Fourier transform infrared (FT-IR) spectra were recorded in transmission mode using a VERTEX 70 spectrometer equipped with a TR module (Bruker, Ettlingen, Germany). Magnetic properties were analyzed using a vibrating sample magnetometer (VSM; Model 8607, Lake Shore Cryotronics, OH, USA). Ultraviolet-visible (UV-vis) absorption spectra were obtained using a V-770 spectrophotometer (Jasco, Tokyo, Japan). Colorimetric measurements were performed using a Ci7600 spectrophotometer (X-Rite, MI, USA).

Author contributions

H. H., M. K., S. K., Y. K., M. S. B., M. H., T. H., and B. H. K. devised the experimental designs. H. H., M. K, S. K., and Y. K. synthesized the nanoadsorbents. M. H., and M. M. prepared the coloured textiles. H. H., M. K., S. K., Y. K., and B. H. K. conducted the dye removal experiments. H. H., M. H., M. S. B, T. H., and B. H. K. wrote the manuscript.

Conflicts of interest

There are no conflicts to declare.

Data availability

The data supporting this article have been included as part of the supplementary information (SI).

The SI includes FT-IR spectra of the nanoparticles, UV–vis calibration curves for the disperse dyes, and measurement details for molecular dimensions of the dyes. See DOI: https://doi.org/10.1039/d5nr03835a.

Acknowledgements

This work was supported by the Korea Institute of Energy Technology Evaluation and Planning (KETEP) and the Ministry of Trade, Industry and Energy (MOTIE) of the Republic of Korea (No. RS-2024-00398166). This work was also supported by the Ministry of Trade, Industry and Energy (MOTIE, Korea) through the Korea Evaluation Institute of Industrial Technology (KEIT) (Project No. 00155462). The work at the Seoul National University was supported by the Research Center Program of the IBS (IBS-R006-D1) in Korea.

References

1 Z. Wang, Y. Tang, L. Zhu, N. Liu, G. Yu, R. Xu, N. Wang, B. Chen and C. Dai, *ChemSusChem*, 2025, **18**, e202402593.
2 X. Fei, H. S. Freeman and D. Hinks, *J. Cleaner Prod.*, 2020, **254**, 120027.
3 J. Lou, L. Ren, J. Yuan, J. Xu, Z. Gu and X. Fan, *Color. Technol.*, 2023, **139**, 338–349.
4 F. Mohtaram and P. Fojan, *Textiles*, 2025, **5**, 24.
5 T. El Darai, A. Ter-Halle, M. Blanzat, G. Despras, V. Sartor, G. Bordeau, A. Lattes, S. Franceschi, S. Cassel, N. Chouini-Lalanne, E. Perez, C. Déjugnat and J. C. Garrigues, *Green Chem.*, 2024, **26**, 6857.
6 M. Imran, B. K. Kim, M. Han, B. G. Cho and D. H. Kim, *Polym. Degrad. Stab.*, 2010, **95**, 1686–1693.
7 Y. Kim, T. Jang, H. Hwang, Y. Sung and B. H. Kim, *Fibers Polym.*, 2025, **26**, 1.
8 T. Huang, X. Wei, S. Qu, W. Zheng and L. Zhao, *J. Supercrit. Fluids*, 2025, **222**, 106607.
9 B. Mu, Y. Shao, L. McBride, H. Hidalgo and Y. Yang, *Resour., Conserv. Recycl.*, 2023, **197**, 107102.
10 E. Sharma, M. K. Hardjopranoto, P. Gunawan, Z. S. Geok Leng, D. T. Chor Yong, N. Gupta, L. Y. Nan and X. Hu, *Clean. Eng. Technol.*, 2025, **27**, 100990.
11 J. Wang, Y. Chen, L. Li, L. Wang and X. Qian, *Iran. Polym. J.*, 2025, **34**, 1221–1230.
12 S. Yi, G. Sun and F. Dai, *Text. Res. J.*, 2018, **88**, 1641–1649.
13 B. Mu and Y. Yang, *Chem. Eng. J.*, 2021, **427**, 131570.
14 H. Zhang, S. Yu, J. Gao, F. Hu, L. Pei, S. Liang, Q. Yang and J. Wang, *Dyes Pigm.*, 2022, **202**, 110264.
15 M. Vaishali, S. Gopal and K. J. Sreeram, *RSC Sustainability*, 2024, **2.8**, 2324–2334.
16 H. Sun, Z. Chen, J. Zhou, L. Chen and W. Zuo, *J. Environ. Chem. Eng.*, 2024, **12.3**, 112558.
17 T. Pradeep, *Thin Solid Films*, 2009, **517**, 6441–6478.
18 S. Joshi, V. K. Garg, N. Kataria and K. Kadirvelu, *Chemosphere*, 2019, **236**, 124280.
19 J. Huang, D. Yan, H. Dong, F. Li, X. Lu and J. Xin, *J. Environ. Chem. Eng.*, 2021, **9.5**, 106277.
20 S. Sun and H. Zeng, *J. Am. Chem. Soc.*, 2002, **124**, 8204–8205.
21 S. Sun, H. Zeng, D. B. Robinson, S. Raoux, P. M. Rice, S. X. Wang and G. Li, *J. Am. Chem. Soc.*, 2004, **126**, 273–279.
22 Y. W. Jun, Y. M. Huh, J. S. Choi, J. H. Lee, H. T. Song, S. Kim, S. Yoon, K. S. Kim, J. S. Shin, J. S. Suh and J. Cheon, *J. Am. Chem. Soc.*, 2005, **127**, 5732–5733.
23 B. Meesaragandla, V. N. K. B. Adusumalli and V. Mahalingam, *Langmuir*, 2015, **31**, 5521–5528.
24 A. Matei, M. Stoian, G. Crăciun and V. Țucureanu, *J. Compos. Sci.*, 2024, **8**, 429.
25 M. Vizcarra-Pacheco, M. Ley-Flores, A. M. Matrecitos-Burruel, R. López-Esparza, D. Fernández-Quiroz, A. Lucero-Acuña and P. Zavala-Rivera, *Polymers*, 2021, **13**, 1791.
26 H. Cho, A. Jin, S. J. Kim, Y. Kwon, E. Lee, J. J. Shin and B. H. Kim, *Materials*, 2024, **17**, 1863.
27 B. H. Kim, W. Ko, J. H. Kim, J. S. Georgiou, M. S. Bootharaju, J. Park and T. Hyeon, *Isr. J. Chem.*, 2025, **65**, e202200103.
28 H. Chang, M. S. Bootharaju, S. Lee, J. H. Kim, B. H. Kim and T. Hyeon, *Bull. Korean Chem. Soc.*, 2021, **42**, 1386–1399.
29 H. Gu, K. Xu, C. Xu and B. Xu, *Chem. Commun.*, 2006, 941–949.
30 M. Colombo, S. Carregal-Romero, M. F. Casula, L. Gutierrez, M. P. Morales, I. B. Bohm, J. T. Heverhagen, D. Prosperi and W. J. Parak, *Chem. Soc. Rev.*, 2012, **41**, 4306–4334.
31 Y. Pan, X. Du, F. Zhao and B. Xu, *Chem. Soc. Rev.*, 2012, **41**, 2921–2942.
32 S. S. Shimo and M. Z. Uddin, *AATCC J. Res.*, 2021, **8**, 15–19.
33 J. Ahmadishoar, H. S. Bahrami, B. Movassagh, H. S. Amirshahi and M. Arami, *Chem. Ind. Chem. Eng. Q.*, 2017, **23**, 21–29.
34 F. M. Kievit and M. Zhang, *Acc. Chem. Res.*, 2023, **56**, 1578–1590.
35 F. Schulz, J. Huhn, M. Werner, D. Huhn, J. Kvelstad, U. Koert, N. Wutke, M. Klapper, M. Froba, V. Baulin and W. J. Parak, *Acc. Chem. Res.*, 2023, **56**, 2278–2285.
36 S. Seth, M. R. Islam, T. Nayak, A. R. Kini, S. Manna, B. K. Malla, A. Nagar and T. Pradeep, *ACS Sustainable Chem. Eng.*, 2025, **13**, 10918–10929.
37 Royal Society of Chemistry, ChemSpider, Chemical Structure 26544, https://www.chemspider.com/Chemical-Structure.26544.html (accessed August 18, 2025).
38 Royal Society of Chemistry, ChemSpider, Chemical Structure 16894, https://www.chemspider.com/Chemical-Structure.16894.html (accessed August 18, 2025).

39 Royal Society of Chemistry, ChemSpider, Chemical Structure 22650, https://www.chemspider.com/Chemical-Structure.22650.html (accessed August 18, 2025).
40 Royal Society of Chemistry, ChemSpider, Chemical Structure 31130, https://www.chemspider.com/Chemical-Structure.31130.html (accessed August 18, 2025).
41 N. Wazzan, *J. Mol. Struct.*, 2009, **920**, 235–242.
42 G. R. Han, D. Hwang, S. Lee, J. Lee, E. Lim, J. Heo and S. K. Kim, *Sci. Rep.*, 2017, **7**, 3863.
43 M. Smith, Z. Li, L. Landry, K. M. Merz and P. Li, *J. Chem. Theory Comput.*, 2023, **19**, 2064–2074.
44 M. Smith, R. Khatiwada and P. Li, *J. Chem. Theory Comput.*, 2024, **20**, 8505.
45 S. A. Blair and A. J. Thakkar, *Chem. Phys. Lett.*, 2014, **141**, 074306.
46 B. H. Kim, K. Shin, S. G. Kwon, Y. Jang, H.-S. Lee, H. Lee, S. W. Jun, J. Lee, S. Y. Han, Y.-H. Yim, D.-H. Kim and T. Hyeon, *J. Am. Chem. Soc.*, 2013, **135**, 2407.
47 M. Feigel, *J. Mol. Struct. (THEOCHEM)*, 1996, **366**, 83–88.
48 J. Huang, D. Yan, H. Dong, F. Li, X. Lu and J. Xin, *J. Environ. Chem. Eng.*, 2021, **9.5**, 106277.
49 J.-S. Kim, E. Kim, K.-M. Lim and E.-B. Cho, *Bioengineered*, 2017, **8**, 99–104.
50 I. Yavari, M. Adib, H. R. Bijanzadeh, M. M. Sadegi, H. Logmani-Khouzani and J. Safari, *Monatsh. Chem.*, 2002, **133**, 1109–1113.
51 J. Huang, D. Yan, H. Dong, F. Li, X. Lu and J. Xin, *J. Environ. Chem. Eng.*, 2021, **9.5**, 106277.
52 J.-S. Kim, E. Kim, K.-M. Lim and E.-B. Cho, *Bioengineered*, 2017, **8**, 99–104.
53 K. Unni, J. S. Kumar, A. Som, D. Sarkar and T. Pradeep, *ACS Sustainable Chem. Eng.*, 2024, **12**, 11957–11967.
54 J. Lou, L. Ren, J. Yuan, J. Xu, Z. Gu and X. Fan, *Color. Technol.*, 2023, **139**, 338–349.
55 M. Li, Y. Li, J. Lu, X. Li and Y. Lu, *Environ. Sci. Pollut. Res.*, 2018, **25**, 34531–34539.